A Froude-scaled model of a bedrock-alluvial channel reach: 1. Hydraulics

Rebecca A. Hodge[1] & Trevor B. Hoey[2]
[1] Department of Geography, Durham University, UK
[2] School of Geographical and Earth Sciences, University of Glasgow, UK

Key points:

1. 3D printing was used to make a 1:10 Froude-scaled flume model of a bedrock channel

2. Velocity, Froude number and Reynolds stress become more spatially variable at higher discharges

3. Velocity correlates with local relief at low discharge and is altered by sediment cover

Abstract

The controls on hydraulics in bedrock-alluvial rivers are relatively poorly understood, despite the importance of the flow in determining rates and patterns of sediment transport and consequent erosion. To measure hydraulics within a bedrock-alluvial channel, we developed a 1:10 Froude-scaled laboratory model of an 18 x 9 m bedrock-alluvial river reach using terrestrial laser scanning and 3D printing. In the reported experiments, water depth and velocity were recorded at 18 locations within the channel at each of 5 different discharges. Additional data from runs with sediment cover in the flume were used to evaluate the hydraulic impact of sediment cover; the deposition and erosion of sediment patches in these runs is analysed in the companion paper. In our data: 1) spatial variation in both flow velocity and Froude number increases with discharge; 2) bulk flow resistance and Froude number become independent of discharge at higher discharges; 3) local flow velocity and Reynolds stress are correlated to the range of local bed topography at some, but not most, discharges; 4) at lower discharges, local topography induces vertical flow structures and slower velocities, but these effects decrease at higher discharges and, 5) there is a relationship between the linear combination of bed and sediment roughness and local flow velocity. These results demonstrate the control that bedrock topography exerts over both local and reach-scale flow conditions, but spatially distributed hydraulic data from bedrock-alluvial channels with different topographies are needed to generalise these findings.

1. Introduction

The reach-scale form and function of river channels is determined by interactions between channel topography, flow and sediment transport. Although these relationships are increasingly well understood in self-formed alluvial channels, they remain poorly defined in bedrock-alluvial channels (bedrock-alluvial encompasses all channels with a predominantly bedrock boundary and any amount of sediment cover, *sensu Turowski et al.*, 2008). Bedrock channels typically erode slowly, so their topography evolves in response to multiple large flow events [*Whipple*, 2004; *Wohl and David*, 2008]; in contrast, alluvial channels can be reconfigured during a small number of events, and within a single event in some cases [*Gupta and Fox*, 1974; *Wells and Harvey*, 1987; *Milan*, 2012]. Consequently, in the context of the relationships between topography, flow and sediment transport, the morphology of bedrock channel boundaries is largely imposed by past conditions and geology, rather than being internally generated in response to the current flow regime. Our aim is to demonstrate how flow and sediment dynamics are controlled by the morphology of the bedrock channel bed, which is static over the timescales of interest and potentially out-of-equilibrium with the flow regime.

This aim is addressed using a Froude-scaled physical model of a bedrock reach, in which key hydraulic and sediment properties are scaled. Channel topography measured in the field using Terrestrial Laser Scanning (TLS) was reproduced at 1:10 scale in a flume using 3D printing. In the flume experiments hydraulics and sediment dynamics were measured across a range of discharges and in runs with sediment supply volumes in a range upwards from zero. This physical model overcomes many of the limitations of field data, such as measuring the spatial pattern of hydraulics and sediment cover under high discharges, and quantifying discharge and sediment supply. This paper focusses on the impact of channel topography on hydraulics, where channel topography encompasses both bedrock topography and surficial sediment cover. A subsequent paper addresses the impact of bedrock topography on the formation and stability of sediment cover.

2. Background and Research Questions

2.1. Feedbacks between morphology, flow and sediment cover

The formative relationships between flow, channel morphology and sediment transport are different between alluvial and bedrock-alluvial systems. In alluvial systems at up to reach scale, adjustments to the channel boundary and bedforms within the timescale of a single event enable the system to respond relatively quickly to changes in external forcing. However, in bedrock-alluvial systems, channel morphology is comprised of both bedrock morphology and sediment cover. These two phases have very different timescales of response; substantial changes in sediment cover can occur during a single event, whereas bedrock erosion typically occurs over far longer timescales and can be considered to be a fixed, independent variable over timescales that are relevant for many geomorphological studies [*Schumm and Lichty*, 1965; *Tinkler and Wohl*, 1998].

The extent to which bedrock morphology is in equilibrium with the current hydrological regime is a function of the erodibility of the bedrock and the frequency of erosion-causing events. Although there are documented examples of significant bedrock incision within individual events [e.g. *Cook et al.*, 2013; *Baynes et al.*, 2015], calculation of a response timescale also needs to account for all the events where erosion does not occur. Consequently, the morphology of a bedrock-alluvial channel reflects the cumulative effect of flow and sediment supply over decades to millennia or longer [*Wohl and David*, 2008]. The current morphology may even reflect a regime that no longer exists, for example a period of enhanced incision has been identified during post-glacial periods of high sediment supply in Scottish rivers [*Jansen et al.*, 2011; *Whitbread et al.*, 2015]. *Wohl and David* [2008] found that bedrock-alluvial rivers exhibit a similar hydraulic scaling between discharge and channel geometry to alluvial rivers, but with the difference that discharge was defined as the largest identifiable event rather than a higher frequency flow, such as mean annual or bankfull discharge, as used in alluvial channels [e.g. *Leopold and Maddock*, 1953]. The recurrence interval of the largest identified discharge is subject to considerable uncertainty, but was estimated as ranging from a few decades to a few centuries. Consequently, bedrock-alluvial channel morphology is likely to be out-of-equilibrium with the more frequent, smaller flow events which are responsible for the majority of sediment transport, and so the relationships between channel morphology and other components of the fluvial system (hydraulics, sediment transport and cover) are likely to be different to those in alluvial systems.

2.2. Hydraulic processes in bedrock-alluvial systems

The interactions between flow and channel morphology in bedrock-alluvial systems reflect the same physical processes as occur in alluvial channels [*Richardson and Carling*, 2006], but there are reasons to expect significant differences in the nature of these interactions between river types. Bedrock-alluvial channels tend to be steeper [*Montgomery et al., 1996*], are more likely to have morphological discontinuities such as knickpoints at a range of scales, often have resistant bedrock walls rather than erodible banks, and are morphologically adjusted to low frequency flow events [*Wohl and David*, 2008]. It has been suggested that bedrock-alluvial channels commonly have flow close to or at critical, with Froude (*Fr*) numbers near or equal to one [*Tinkler and Wohl*, 1998], although super-critical flows have been identified under high discharges [*Turowski and Rickenmann*, 2009] and in steep reaches. Clustering around *Fr* = 1 suggests a form of internal hydraulic regulation associated with energy dissipation, consistent with suggestions that critical flow can become a controlling factor in streams where width is constrained [*Huang et al.*, 2004].

Field observations in bedrock-alluvial channels indicate that flow resistance initially decreases with increasing discharge, before stabilising at a higher discharges [e.g. *Richardson and Carling*, 2006; *Heritage et al.*, 2004; *Van et al.*, 2012]. Very low discharges are characterised by non-uniform flow, with alternating pools and supercritical flow over bedrock steps [*Richardson and Carling*, 2006]. Energy is dissipated by hydraulic jumps, internal distortion in the flow and the physical roughness of bedrock outcrops [*Heritage et al.*, 2004; *Van et al.*, 2012]. As discharge increases, flow becomes more uniform, with few dead zones and a progressive increase in *Fr* and decrease in flow resistance. *Richardson and Carling* [2006] termed this state the macroturbulent mixing state (MMS), which is characterised by frequent eddy shedding from irregularities in the channel bed and high turbulent intensities as the area of the bed wetted by the flow progressively expands. The MMS is fully established at a threshold discharge above which there is no further decrease in flow resistance.

At higher discharges, *Richardson and Carling* [2006] identified a second state, where the flow separated into a central core of critical flow with marginal slack water zones, termed the decoupled dead zone state (DDZS). The switch occurred concurrently with the flow asymptotically approaching *Fr* = 1, suggesting that that development of a shear layer provides internal regulation that prevents the flow from becoming supercritical [*Tinkler*, 1997]. *Venditti et al*. [2014] identify similar 3D turbulent structures related to longitudinal discontinuities in the beds of bedrock canyons. Another possible mechanism, hypothesised by *Grant* [1997], is that flows asymptotically approach *Fr* = 1 because of interactions between the free surface and channel bed; small irregularities in the bed surface produce hydraulic jumps and surface waves, which rapidly dissipate energy. Wall undulations may play a similar role [*Wohl et al.*, 1999], with *Richardson and Carling* [2006] suggesting the decoupling they observed could be caused by the relatively rougher channel side walls starting to become submerged. One apparent contradiction is that these energy dissipation mechanisms are equivalent to a progressive increase in flow resistance with stage, yet field measurements suggest that this is more than compensated by drowning out of bed roughness as flow stage rises. The extent to which these different states are generally found in bedrock-alluvial channels remains to be assessed.

2.3. Hydraulic data from bedrock-alluvial systems

The ability to address questions around channel hydraulics and changing flow resistance is limited by the availability of hydraulic data from bedrock-alluvial channels. Since *Tinkler's* [1997] velocity data from a single cross-section at different discharges, very few comparable datasets have been collected. *Venditti et al.* [2014] present high resolution hydraulic data from a series of bedrock canyons to analyse the flow structures induced by the lateral constriction of the canyons, giving specific findings that are not applicable to a broader range of bedrock-alluvial channels. Similar limited generality applies to hydraulic data from flume experiments. For example, the experiments of *Johnson and Whipple* [2010] and *Finnegan et al.* [2007] were based on a self-formed channel that tended to evolve into a tortuous slot canyon, with the shallow flows making hydraulic measurements difficult. Other flume experiments have only recorded reach-average conditions [*Chatanantavet and Parker*, 2008; *Inoue et al.*, 2014]. Finally, flume experiments tend to have far higher *Fr* numbers than are hypothesised to occur in natural bedrock-alluvial channels; example reported flume *Fr* numbers are 2.4 to 3.5 [*Johnson and Whipple*, 2010], ~ 1.4 [*Finnegan et al.*, 2007], and up to 2.4 [*Chatanantavet and Parker*, 2008]. These limitations mean that there is therefore a need for spatially distributed datasets of hydraulic measurements from bedrock-alluvial channels with which to assess their behaviour.

2.4. Hydraulic processes, bedrock roughness and sediment cover

The previous work discussed above addressed changes to reach-scale hydraulics as a function of discharge, but did not try to quantify the impact that a particular channel topography has on the hydraulics. Even at the reach-scale, it is still unclear how the roughness (a measure of the bed topography) and flow resistance (calculated from hydraulic data) of a bedrock-alluvial channel should be quantified, and how these properties change as sediment patches develop. Different methods have been proposed for quantifying channel topographic roughness. In flume experiments, *Johnson and Whipple* [2007, 2010] and *Finnegan et al.* [2007] used the standard deviation of elevations relative to a plane fitted to the surface. This physically meaningful property [*Coleman et al*, 2011] appeared to correlate with the development of sediment cover and channel incision. An alternative flow resistance approach back-calculates a roughness length from hydraulic data (typically average depth and velocity) and a relationship such as the Manning-Strickler formula [*Chatanantavet and Parker*, 2008; *Johnson*, 2014]. However, *Chatanantavet and Parker* [2008] and *Inoue et al.* [2014] found that there was not a good correlation between the roughnesses obtained from topographic and flow resistance methods for different surfaces. These data therefore question the extent to which a single topographic index records the influence of the bed morphology on the flow.

Attempts to quantify bed roughness and flow resistance are further complicated by the development of sediment cover. *Johnson* [2014] and *Inoue et al.* [2014] both developed approaches for calculating the roughness of a bedrock-alluvial surface. *Johnson* [2014] calculated total roughness as an area-weighted mean of the roughness of the alluvial component, determined from grain size, and the bedrock component, estimated as the standard deviation of surface elevations. *Inoue et al.* [2014] used a similar approach, although they assumed a linear transition between bedrock and alluvial roughness as the sediment cover infills the bed topography. Despite the importance of this issue for predicting sediment cover dynamics, these estimates have not been robustly tested using topographic and hydraulic data. Such testing again requires a spatially distributed dataset of hydraulic properties from a bedrock-alluvial channel with known topography.

2.5. Research questions

This research begins to address some of the gaps in current knowledge identified above using flow data from a 1:10 scaled model of a bedrock-alluvial reach. The specific questions that the data are used to answer are:

1. How do the spatial patterns of hydraulic properties change with discharge?
2. To what extent does local bed topography affect velocity?
3. How do sediment patches affect local hydraulics?

These experiments are the first example of which we are aware of a Froude-scaled model of a prototype bedrock-alluvial channel. As the prototype site has *Fr* close to 1 at high flows, these experiments thus provide a data set for addressing competing ideas on the development of reach-scale hydraulics that is complementary to the supercritical *Fr* numbers of previous flume models [e.g. *Chatanantavet and Parker,* 2008; *Johnson and Whipple*, 2010]. The spatially distributed nature of the velocity measurements across a range of discharges begins to overcome the limitations of reach-averaged approaches used previously.

3. Methods

3.1. Field Methods

The prototype is an 18 m long reach of Trout Beck, North Pennines, UK (54°41’35’’N 2°23’18’’W), which has an average width of 9 m, gradient of 0.02, and 22% sediment cover. The bedrock is Alston Formation Limestone, and the channel bed has a blocky topography with approximately horizontal bedding ~ 0.5 m thick, preferential erosion along vertical joints and vertical relief of up to 1 m (Figure 1). Unlike some bedrock channels, there is no inner channel (Figure 1). Sediment D_{16}, D_{50} and D_{84} are 23, 70 and 146 mm, respectively (where D_x is the grain size for which x% is finer). Although the study reach does not have the extreme topography of some bedrock-alluvial channels, its topography is representative of many other channels (e.g. images in *Tinkler and Wohl,* 1998; *Inoue et al.*, 2014; *Whitbread et al.*, 2015].

Flow data were measured at low to moderate flows, and extrapolated to discharges equivalent to those used in the flume. Discharge (Q) was measured using dilution gauging [*Elder et al.*, 1990] and mean depth ($\overline{h}$) by measuring the water surface level at eight surveyed cross sections within the reach. Reach-averaged mean velocity ($\overline{U}$) was obtained from $\overline{U}$ = $Q/\overline{A}$ and $\overline{A} = \overline{h}\ \overline{w}$, where A is wetted cross-section area and w is flow width. Depth and velocity at higher discharges were estimated in the same way but using water levels determined from stage-discharge rating curves at two pressure transducers, one 58 m upstream of the reach and one at the downstream end of the reach.

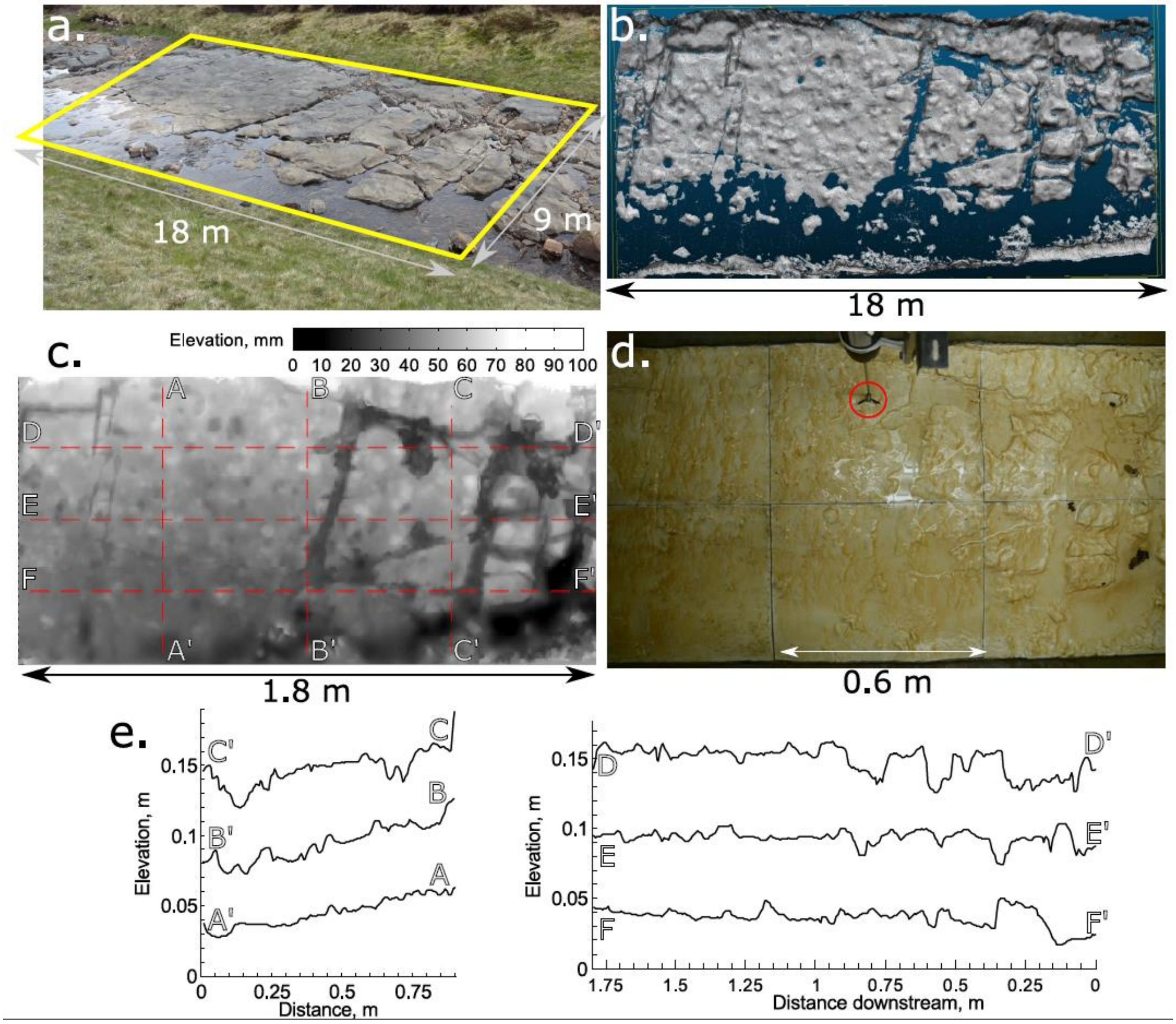

Figure 1: a. Trout Beck, with experimental area identified. b. Terrestrial Laser Scanning (TLS) point cloud. Gaps indicate areas covered with water, infilled using differential GPS (dGPS) survey. c. Digital elevation model created from TLS and dGPS data. Letters and dashed lines correspond with transects shown in panels e and f. d. Printed tiles installed in the flume. Acoustic Doppler Velocimeter (circled) shown in position for experimental runs with sediment. e. Cross-sections and long profiles of the tiles. All elevations have had the flume slope removed and so are relative to the sloping flume bed. Sections are plotted with a five times vertical exaggeration. For clarity, sections B and E are vertically offset by 0.05 m, and sections C and D by 0.1 m. The 18 measurement positions were located along the three cross-sections. Flow is right to left.

The bed topography of Trout Beck was surveyed using TLS under very low flow conditions. Scan data were collected from four different positions at a point spacing of up to 5 mm at the centre of the channel. The combined TLS data were trimmed to the area of interest and obviously erroneous points were removed manually. The resulting TLS data had an average density of 33,000 points m^{-2}. Differential GPS (dGPS) was used to survey the 29% of the bed that was underwater and therefore not represented in the TLS data, with an average point density of 43 points m^{-2}. Existing sediment cover was left within the reach during the survey.

TLS and dGPS data were processed to produce 3D tiles suitable for printing. See Supplementary Material for further details of the methods. The banks of Trout Beck are close to vertical; the banks in the flume were its vertical glass walls.

3.2. Flume Methods

Experiments were conducted in the 0.9 m wide flume at the University of Glasgow, UK. This has a working length of 8 m and maximum discharge of 75 l s^{-1}. In order to replicate field processes in the flume, the experiments were Froude scaled with a length scale of 1:10. Following Froude scaling convention, the flume slope is the same as the field (0.02), the length scale λ_x applies to width, depth and sediment size, velocity scales as $\lambda_x^{0.5}$ and discharge as $\lambda_x^{2.5}$ [*Young and Warburton*, 1996; *Thompson and Wohl*, 1998].

Tiles were fixed to the bed of the flume 3.5 m from the upstream end. The root mean square of the differences between measured and expected elevation at 30 locations across the tiles was 3.6 mm, with a range of 10.8 to 0 mm, indicating limited tile warping during printing and installation. At the upstream edge of the tiles, the space between their irregular surface and the flume bed was filled with a vertical acrylic sheet cut to shape, to prevent flow from getting under the tiles and generating lift. Coarse uniform sediment (D_{50} ~ 16 mm) was used to fill the rest of the flume to a level equal to the top of the tiles to ensure development of a turbulent flow profile before flow reached the tiles and to inhibit scour downstream of the tiles. There was little movement of this sediment during the experiments. This sediment size is comparable to the standard deviation of elevations of the modelled section (12 mm), and so on entering the tiles the flow is already adjusted to a surface of a comparable roughness, albeit with less large scale structure.

Flow was smoothed by a baffle plate in the header area, and depth was controlled by a tailgate set to avoid backwater development at low flow. Flow depth profiles measured along the side of the flume indicated that flow became uniform a short distance (<2 m) downstream of the entrance, and was maintained until the top of the tiles, at which point it became strongly non-uniform. As our field conditions had *Fr* close to one, we avoided many of the problems associated with strongly sub-or super-critical flow. Backwater effects from the flume tailgate did not propagate as far upstream as the tiles.

Two main sets of experiments were undertaken: the first used clear water conditions to measure the variable impact of the topography on the flow; in the second, different volumes of sediment were supplied to measure the impact of the topography on sediment patch dynamics, and any consequent impacts on the flow. The second set is primarily reported in the companion paper [*Hodge and Hoey, in review*]. In the first set, discharge was set to one of a series of constant values between 20 and 60 l s^{-1}. 20 l s^{-1} is equivalent to just below bankfull in the field setting. For each run, flow depths were measured along the smooth glass side of the flume. Width-to-depth ratios are greater than 12, indicating that wall induced circulation will be minimised [*Colombini*, 1993]; these low friction walls are expected to increase velocities close to the channel margins compared to the field situation. A Sontek 10MHz micro-Acoustic Doppler Velocimeter (ADV) was used to record 3D flow velocities at 25 Hz for 3 minutes at each of 18 locations across the tiled section. The instrument measurement volume is 4 mm in diameter with a height of 4.5 mm. Local flow depth was measured at each location using a point gauge. Flow velocities were measured at a constant height to record near bed flow conditions, which are important for sediment dynamics as discussed in the companion paper. To ensure that the ADV did not come into contact with the bed at any of the measurement locations, this height was 15 mm above the bed. At two locations downstream bed topography prevented the ADV from being placed so close to the bed, so flow here was measured at heights of 19 and 23 mm (second from right in top transect and third from right on middle transect, respectively).

In the second set of experiments (described in detail in *Hodge and Hoey* [*in review*]), fixed masses of sediment were introduced into the flume under constant flow conditions, including a control run with zero sediment input. After 5 minutes during which sediment formed stable configurations on the bed, the discharge was gradually increased at 0.7 l min^{-1} up to a maximum value of ~ 70 l s^{-1} to determine erosion thresholds for sediment in different locations. ADV data were collected at 25 Hz for the duration of the experiment at a fixed location (Figure 1). These time series were split into 3 minute intervals for analysis. Vertical photographs centred on the mid-point of the tiles, from which sediment cover was quantified, were taken every 5 seconds throughout the experiment. The extent of sediment cover around the ADV measurement volume was calculated for each run, where the analysed area extends 20 mm either side of the centre of the ADV, and 50 mm upstream. The lateral distance is ~ 1.4 D_{84} and the upstream distance is ~ 3.5 D_{84}; for comparison, research on the influence of pebble clusters on flow suggests little lateral influence beyond the extent of the grain, but a downstream influence of up to 3.5 times obstacle height [*Brayshaw et al.*, 1983; *Lawless and Robert*, 2001; *Lacey and Roy*, 2008]. Sediment cover developed in the analysed area of the bed in seven out of the 13 experiments with sediment.

3.3. Velocity data

The shallow, turbulent flows meant that standard filtering thresholds for processing ADV data [*Lane et al.*, 1998] were not applicable because the data displayed relatively low correlation values [*Strom and Papanicolaou*, 2007]. In turbulent flows, *Wahl* [2000] suggests that points with a correlation of < 0.7 can still provide good data if the signal-to-noise ratio (SNR) is high. The ADV data were initially filtered using a correlation threshold of 0.4 [*Martin et al.* 2002, *Strom and Papanicolaou* 2007], a signal to noise (SNR) ratio of 10 [*Wahl*, 2000; *Strom and Papanicolaou*, 2007] and the expected measurement range. Further removal of spikes caused by aliasing was achieved by removing all velocity measurements that fell outside three standard deviations of the mean, and then recalculating and repeating this step once [*Buffin-Belanger et al.*, 2006; *Doroudian et al.*, 2010].

All data were initially inspected by plotting the time series, and by plotting the different velocity components against each other. Of the 90 time series from the first set of experiments (5 discharges by 18 positions), 13 were rejected on the basis of the proportion of points that were removed, and/or the presence of aliasing or spikes in the filtered data. For the second set of experiments, one of the 14 runs was removed after processing because aliasing still appeared to be present in the data. The retained time series were used to calculate the mean velocity and root-mean square of velocity fluctuations, Reynolds stress and turbulent kinetic energy per unit mass (TKE). We use the labelling convention U (downstream), V (vertical), and W (cross stream). To normalise the velocity data we use the shear velocity, $U^* = (g \overline{h} S)^{0.5}$, where g is gravitational acceleration, S is flume slope (0.02), and $\overline{h}$ is the average flow depth at the 18 locations [*Babaeyan-Koopaei et al.*, 2002; *Legleiter et al.*, 2007].

For the first set of experiments, the 13 rejected time series had poor quality vertical velocity data. However, mean velocities were calculated using the downstream and cross-stream components of these data series. Analysis of the downstream and cross-stream components for these 13 series used the same filtering process as outlined above, but only removed identified points from one, rather than all three, directions. Comparison of mean velocities from data filtered using the two different approaches had a RMS error of 0.015 and 0.006 m s^{-1} in the downstream and cross-stream directions, respectively.

4. Results

We start by demonstrating that the flume is a scaled representation of the field conditions. We then present the hydraulics of the flume at the 18 measurement locations, and consider how they vary with discharge. The spatial distribution of hydraulic properties is then presented, followed by an analysis of the relationships between different topographic indices and local flow conditions. We end by assessing the impact that sediment patches have on local hydraulics.

4.1. Model Froude Scaling

Reach-averaged field data are used for direct comparison of hydraulic variables from the field and the flume, as no point measurements are available from the field site. Hydraulic scaling relationships are used to test the consistency of reach-averaged Froude number, water depth, velocity and flow resistance (Darcy-Weisbach friction factor, f) between the model and field across the range of modelled discharges. Figure 2 demonstrates that the field and flume data fall along power law relationships between each of these variables and discharge, which is consistent with standard hydraulic geometry relationships [*Leopold and Maddock*, 1953]. Data extrapolated from the field measurements to high discharges show good agreement with the scaled flume data, particularly for velocity and flow resistance. The small offset for depth is consistent with the effect of the flume having a fixed width, whereas the prototype width changes by approximately 10% with discharge.

Reynolds numbers averaged across the flume and at each of the 18 measurement locations are all >> 2000, indicating fully turbulent flow. Particle Reynolds numbers ($Re^* = U^* D_x / \nu$ where D_x is a length scale based on the xth percentile of the grain size distribution and ν is the kinematic viscosity of water at the laboratory temperature) for D_{50} are > 70 at all discharges. Using D_{16} as a much more conservative estimate of roughness Re^* is also > 70 at all discharges. Furthermore, with much finer sediment, a lower threshold Re^* of 15 has been proposed [e.g. *Peakall et al.*, 1996]. Consequently, nearly all grains are experiencing rough turbulent flow and sediment transport processes can be considered to be dynamically similar to the prototype [*Young and Warburton*, 1996].

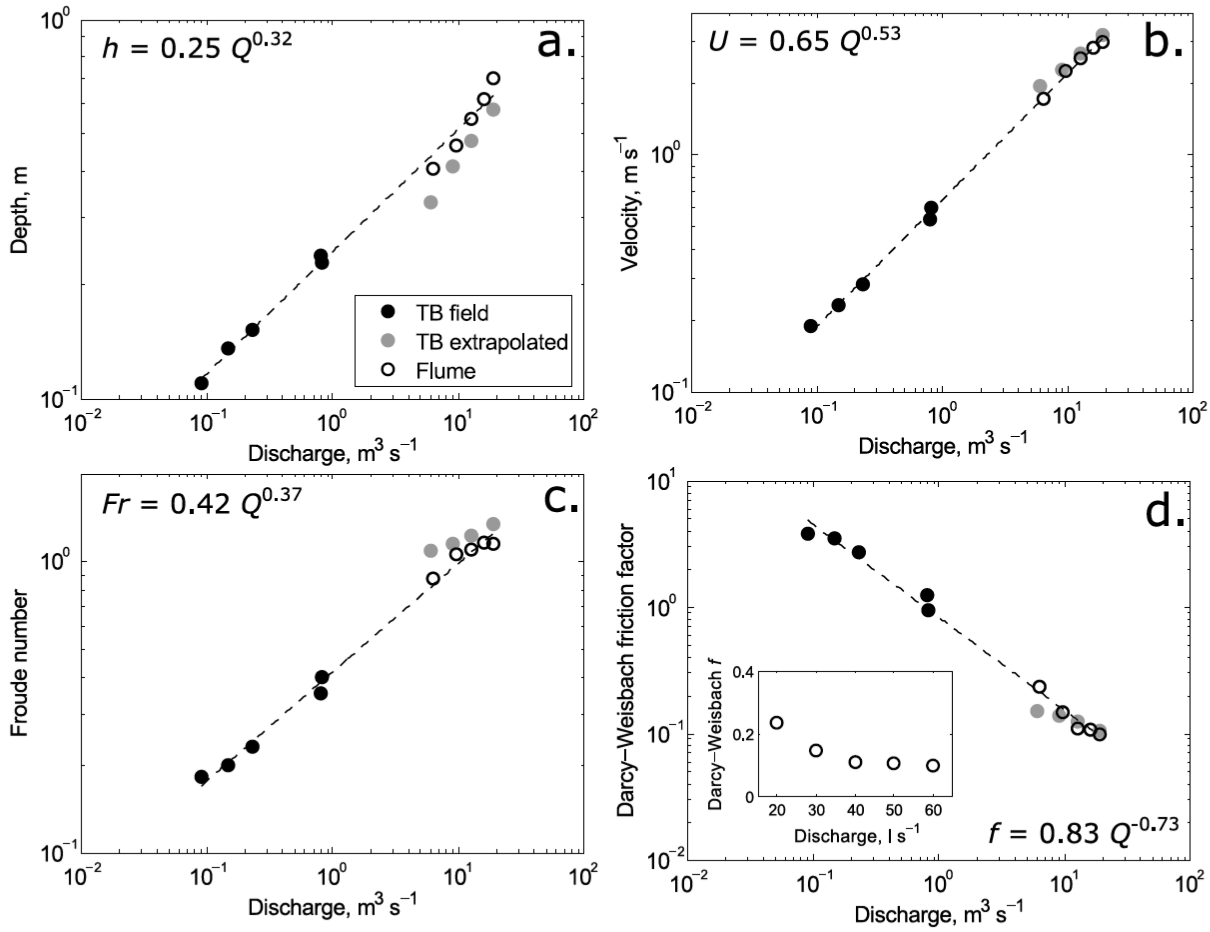

Figure 2: Comparison of calculated reach-averaged a) depth (h), b) velocity (U), c) Froude number (Fr) and d) Darcy-Weisbach friction factor (f) from the field site Trout Beck and from these flume experiments. Flume data are scaled to field dimensions. Two sets of field data are presented. TB field are data collected during low flow conditions using salt dilution gauging. Field data from higher discharges are unavailable due to the difficulty of measuring in high flow. TB extrapolated are values extrapolated from the low flow conditions to higher discharges. Flume data are from the range of discharges used in this study; data from lower discharges are unavailable due to the difficultly of measuring very shallow flows. Flume flow depths are the average from the 18 positions where ADV data were collected. Average velocity is calculated from the bulk discharge and this average flow depth. Dashed lines show power law regressions to the flume and TB field data. All regression R^2 values are > 0.99, and 95% confidence intervals on all coefficients and exponents show that they are significantly different to zero. Inset in d) shows just the relationship for flume data using the original flume dimensions.

4.2. Changes in hydraulics as a function of discharge

As discharge rises from 20 to 60 l s^{-1} water depth increases linearly (Figure 3a), whereas mean downstream velocity increases more rapidly at lower discharges than at higher discharges (Figure 3b). There is considerable spatial variation in depth and velocity across the channel bed. The range of depths is approximately constant at all discharges (43 mm at 20 l s^{-1} to 49 mm at 60 l s^{-1}), whereas the range of downstream velocity increases with increasing discharge (range of 0.53 m s^{-1} at 20 l s^{-1} to 0.77 m s^{-1} at 60 l s^{-1}). Data from individual locations can vary from the overall trend, with up to 28% of the locations showing decreases in depth or velocity as discharge increases. Decreases are slightly more likely for velocity rather than depth. Flow resistance (Darcy-Weisbach friction factor) decreases with increasing discharge up to Q = 40 l s^{-1}, then remains fairly constant up to Q = 60 l s^{-1} (Figure 2d inset).

At all discharges, there are some locations with supercritical flow (Figure 3c), the proportion of which increases from 8 to 12 (of 18 locations) as discharge increases from 20 to 60 l s^{-1}. The mean value of *Fr* increases from 0.88 ± 0.07 (one standard error) at 20 l s^{-1} to 1.05 ± 0.08 at 30 l s^{-1} before stabilising at 1.09 ± 0.08 or 1.10 ± 0.08 at 40 to 60 l s^{-1}. As with depth and velocity, *Fr* number at a location can decrease, as well as increase, with increasing discharge.

Reynolds stress (Figure 3d) shows a similar pattern to the other properties, increasing from a mean of 1.0 to 3.1 N m^{-2}. There is less variation in TKE, the average of which increases by about 30% from 16.0 J kg^{-1} at 20 l s^{-1} to 21.4 J kg^{-1} at 60 l s^{-1}. In contrast, quadrant analysis of the velocity data indicates some change in the flow structures with changing discharge. The mean proportion of the time that the ADV data are in quadrants 2 and 4 (ejections and inrush events) is fairly constant (52% at Q = 20 l s^{-1} to 55% at Q = 60 l s^{-1}), but the range increases with increasing Q (Figure 3e), indicating that the flow appears to be becoming more spatially variable. As with previous flow properties, at each location the proportion of Q2 and Q4 events can increase or decrease at a higher discharge.

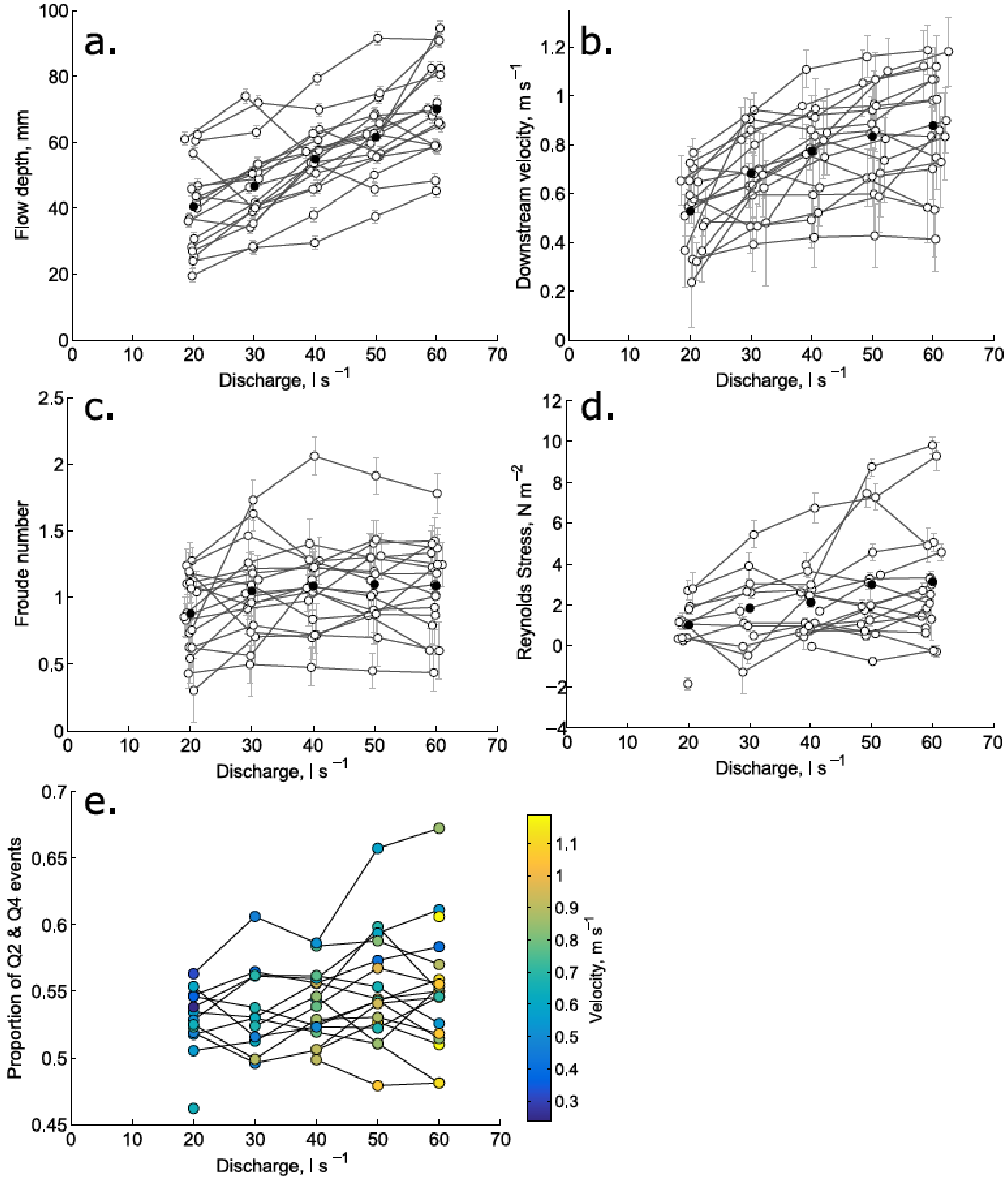

Figure 3: Increase in a) flow depth, b) downstream velocity, c) point Froude number and d) point Reynolds stress with increasing discharge in clear water runs. In a) black points are the mean flow depth. Measurement errors are ± 2 mm. In b) velocity is measured at an elevation of 15 mm for most locations. Black points are the mean downstream velocity. Error bars are one standard deviation of the ADV measured velocities; error bars of one standard error of the mean plot within the circular markers. In c) black dots are average Froude numbers. Error bars are calculated using ± one standard deviation of the velocity measurements. In d) black dots are average Reynolds stresses. Error bars are one standard error of the mean. e) shows the proportion of turbulent flow events in quadrants 2 and 4 (ejections and inrush

events). Point colours indicate mean downstream velocity. In all plots apart from e), points are jittered about the x-axis value for clarity.

To aid comparison between the different discharges, mean flow velocities and RMS values were normalised by *U** at each discharge (Figure 4). For most components of the velocity the normalised data from different discharges collapse onto the same trend, showing that there is a consistent structure to the flow across the discharges. The main exceptions to this pattern are for *U*/*U** and RMS_V/U^*. At 20 l s^{-1}, the values of *U/U** are significantly lower than at the other four discharges (Kruskal-Wallis test, $p = 0.063$). For RMSv/U* there is a systematic decrease in range and values as discharge increases (Kruskal-Wallis test, $p < 0.001$). In summary, downstream velocities are lower than expected at 20 l s^{-1}, and the vertical mixing in the flow decreases with increasing discharge. *Legleiter et al.* [2007] report similar data from an alluvial channel (D_{50} = 124 mm) under low flow conditions. Comparing the range of their results to those in Figure 4, we find that our results typically have a larger range for all components, with the exception of *W*/*U**.

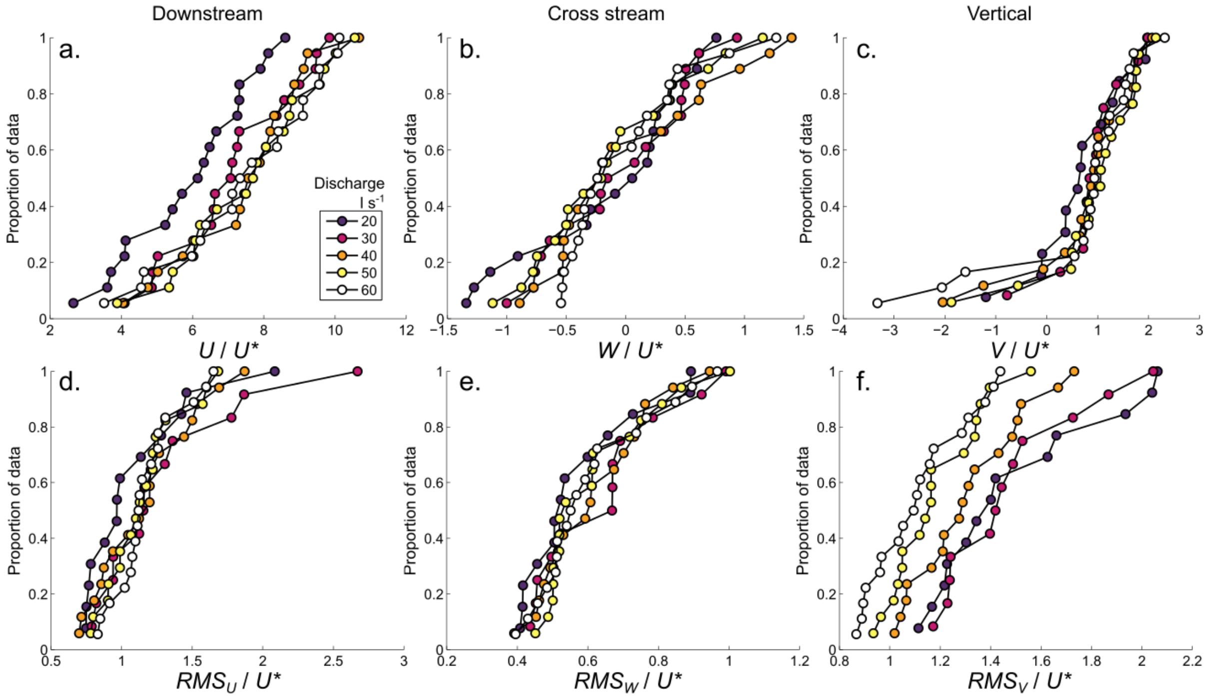

Figure 4: a to c) Distributions of mean U (downstream), W (cross stream) and V (vertical) velocities for all 18 measurement locations at all 5 discharges. d to f) Distributions of the RMS of velocity fluctuations. All data are normalised by U to enable comparison between different discharges.*

4.3. Spatial patterns of hydraulics

Vectors of planform velocity (Figure 5) are predominantly downstream at all discharges, with small cross-stream components suggesting limited transverse topographic steering. The range of velocities is always greatest in the upstream transect, which has the most topographic variation (Figure 1e). At Q = 20 l s^{-1}, higher flow velocities occur in the centre of the upstream and downstream transects, with lower than average velocities across the middle transect. As discharge increase, velocities increase fastest in the middle transect, linking together high velocity areas in the upstream and downstream transects and creating a high velocity pathway through the model reach. Consequent on the velocity changes, areas of supercritical flow become connected as discharge increases.

Reynolds stress is more varied than velocity across the model (Figure 6), and shows a similar spatial pattern at all discharges, although the range of values increases with discharge. Consequently, areas of high Reynolds stress do not become connected. As with velocity, Reynolds stress is more variable in the upstream transect with the greatest relief. Higher values of Reynolds stress are typically, but not always, associated with higher values of RMS_U.

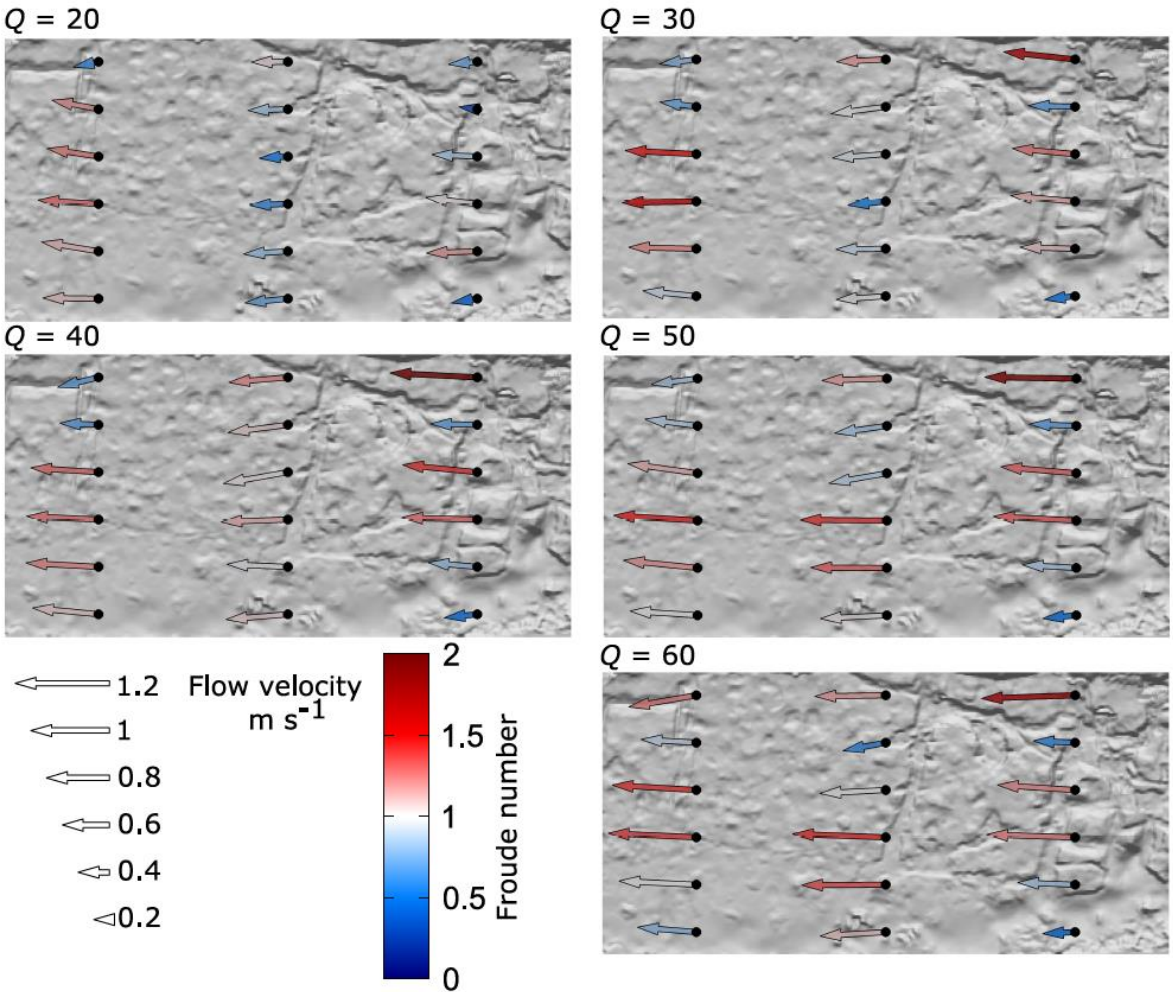

Figure 5: Vectors of down- and cross-stream velocity under five different discharges (Q) between 20 and 60 l s^{-1}. Arrow lengths show magnitude of resultant velocity, with all plots using the same scale. Arrow colours show local Froude number. Black dots show the measurement locations.

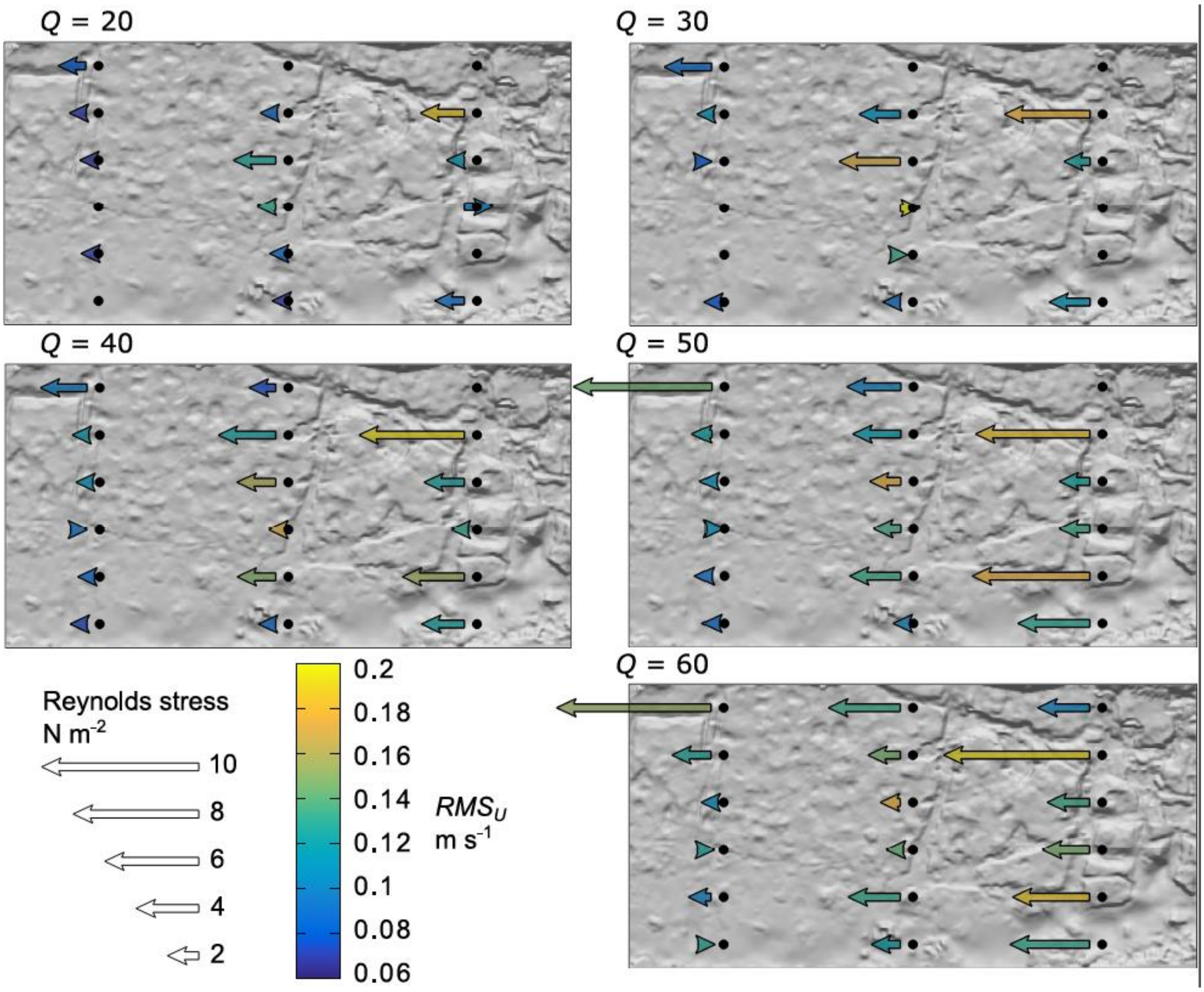

Figure 6: Maps of average Reynolds stress (arrow length) and RMS_U (colours) at each of the different discharges (Q). Upstream pointing arrows are negative Reynolds stresses. Absent arrows indicate that ADV data was not of sufficient quality to calculate Reynolds stress. Black dots show the measurement locations.

4.4. Relationships between bed topography and local hydraulics

Figure 7 shows the extent to which the local bed elevation accounts for the variation in flow depth and velocity. Unsurprisingly, flow depth shows an inverse relationship with bed elevation; this relationship is fairly consistent across all discharges suggesting that there are not large changes in the water surface slope over the range of imposed discharges (Figure 7a). Because of the momentum of the flow, velocity is not expected to show a strong correlation with either local elevation or flow depth, as seen in Figure 7b and c.

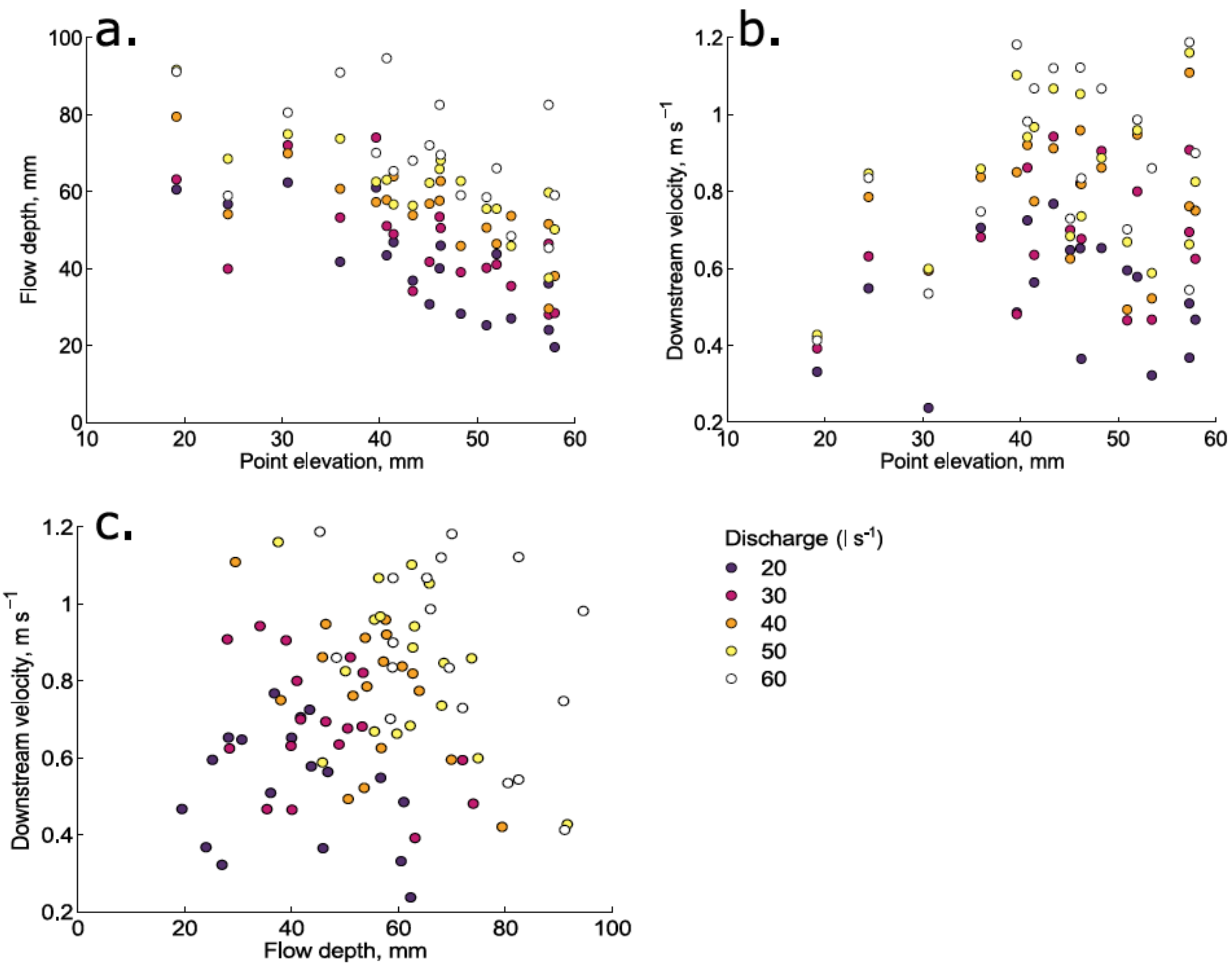

Figure 7: Relationships between downstream velocity, bed elevation and water depth across all five discharges at each of the 18 measurement locations.

To determine the length scales over which bed topography does affect the flow velocity, we regress measures of the bed topography against velocity and Reynolds stress from the 18 measurement locations. We use two different indexes of bed topography. Firstly, the maximum difference in elevation between the measurement point and the upstream bed over a given distance (Δ_z). For this calculation we consider the bed elevations over a lateral width of ± 30 mm to account for possible lateral deflection of the flow. This lateral width value produced relationships with the highest R^2, but its exact value does not make a significant difference to the overall findings. Secondly, we calculate the standard deviation of elevations of the local bed topography (σ_z) [*Inoue et al.*, 2014; *Johnson*, 2014], calculated over a square area centred on the measurement location. Both Δ_z and σ_z require a length scale over which the index is calculated. One approach would be to identify the smallest scale at which these indexes reach a constant value. However. because of the irregular bed topography, the value of σ_z depends on the size of the area of bed elevations. Figure 8 shows that the distribution of σ_z does not stabilise as the window size increases up to the width of the flume, suggesting that there is not a geometrically optimum window size to apply. Consequently we use a range of sizes.

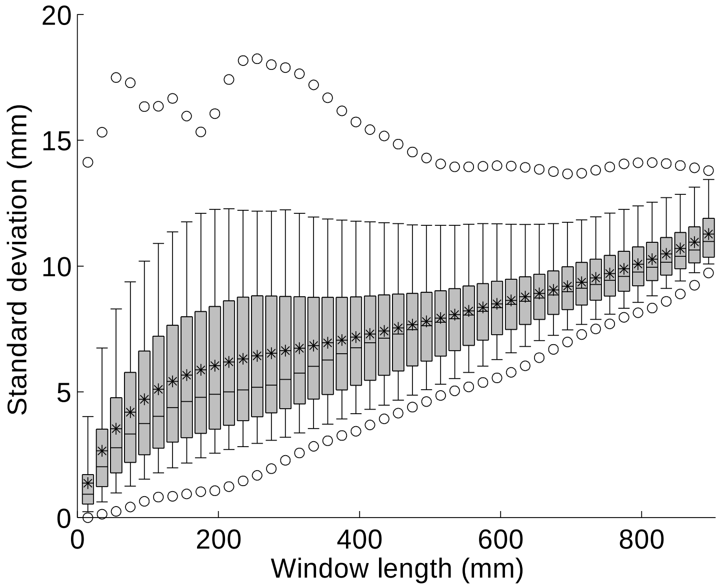

Figure 8: The standard deviation of the bedrock topography calculated using a square moving window of increasing length. Boxplots show the minimum and maximum values (o), 5th and 95th percentiles (whiskers), 25th, 50th, and 75th percentiles (box and dashed line), and mean (*). Lengths are for the flume tiles; multiply by ten to get length scales for the field.

For each discharge, linear regression was used to analyse the relationship between: 1) U and Δ_z; 2) Reynolds stress and Δ_z, with Δ_z calculated over a range of upstream distances in both cases; and, 3) U and σ_z calculated using a range of window sizes. For each of these combinations multiple regression was also conducted, including the measurement point elevation (z) in addition to the topographic index (Δ_z or σ_z). Linear regressions between the hydraulic parameters and the measurement point elevation (z) were also undertaken.

Regressing velocity against these topographic indices is supported through analysis of flow resistance equations. A linear relationship between σ_z and velocity would result from Manning's n being proportional to topographic roughness. In the case of the Darcy-Weisbach equation, standard hydraulic relationships are:

$$\tau = \rho g h S \qquad (1)$$

$$U^2 = 8ghS/f \qquad (2)$$

$$f = 8\Big/\left[a_0^2\left(\frac{h}{k}\right)^{1/3}\right] \qquad (3)$$

where a_0^2 is a coefficient with a value of 8 [*Ferguson*, 2012], k is a representative roughness length, and ρ is the density of water. Rearranging equations (1, 2 and 3) gives $U \propto k^{-1/6}$.We therefore show both linear and power law fits to the strongest relationship between the hydraulic and topographic parameters in Figure 9.

Figure 9 shows how the R^2 values of the different relationships vary with both upstream distance/window size and discharge. For the relationships between U and Δ_z or σ_z, the highest, significant ($p < 0.05$), correlations occur at a discharge of 20 l s^{-1}. Relationships using Δ_z

produce higher R^2 than those using σ_z indicating that the flow responds to steps in the bed topography, rather than to the average bed roughness. Plots of the relationships with the highest R^2 show the expected negative correlation (Figure 9b and f). The highest R^2 values are given by relationships that incorporate both z and either Δ_z or σ_z; however, relationships using only Δ_z or σ_z are significant, whereas those using only z are not. Consequently, although relationships using only z are very weak, z does add explanatory power when included in a multiple regression with other variables. At a discharge of 20 l s^{-1} there is a rapid increase in R^2 between length scales of 110 and 205 mm (Figure 9a), with maximum R^2 occurring at 295 mm. In Figure 9e maximum R^2 occurs at a window size of 300 mm.

At higher discharges the relationship between U and Δ_z or σ_z is not significant, with the exception of that between U and Δ_z when Q = 30 l s^{-1}. At discharges greater than 20 l s^{-1} in Figure 9a there is relatively little difference between the relationships using Δ_z, Δ_z and z, and just z, indicating that each variable can explain comparable small amounts of the variation in U. In contrast, in Figure 9e, relationships using σ_z and z, or just z, have a comparable R^2, but those using σ_z have a far smaller R^2. Consequently σ_z is a poor predictor of U at these discharges.

Relationships between Δ_z and Reynolds stress show a different relationship. Significant relationships occur at discharges of 30 and 60 l s^{-1}, with a positive correlation between the topographic index and the Reynolds stress (Figure 9c and d). The R^2 is mostly accounted for by Δ_z, with the addition of z adding some explanatory power. Relationships using z alone have a very low R^2. The highest R^2 values occur at similar topographic length scales to those in Figure 9a, at upstream distances of 250 mm and 200 mm when Q = 30 and 60 l s^{-1} respectively.

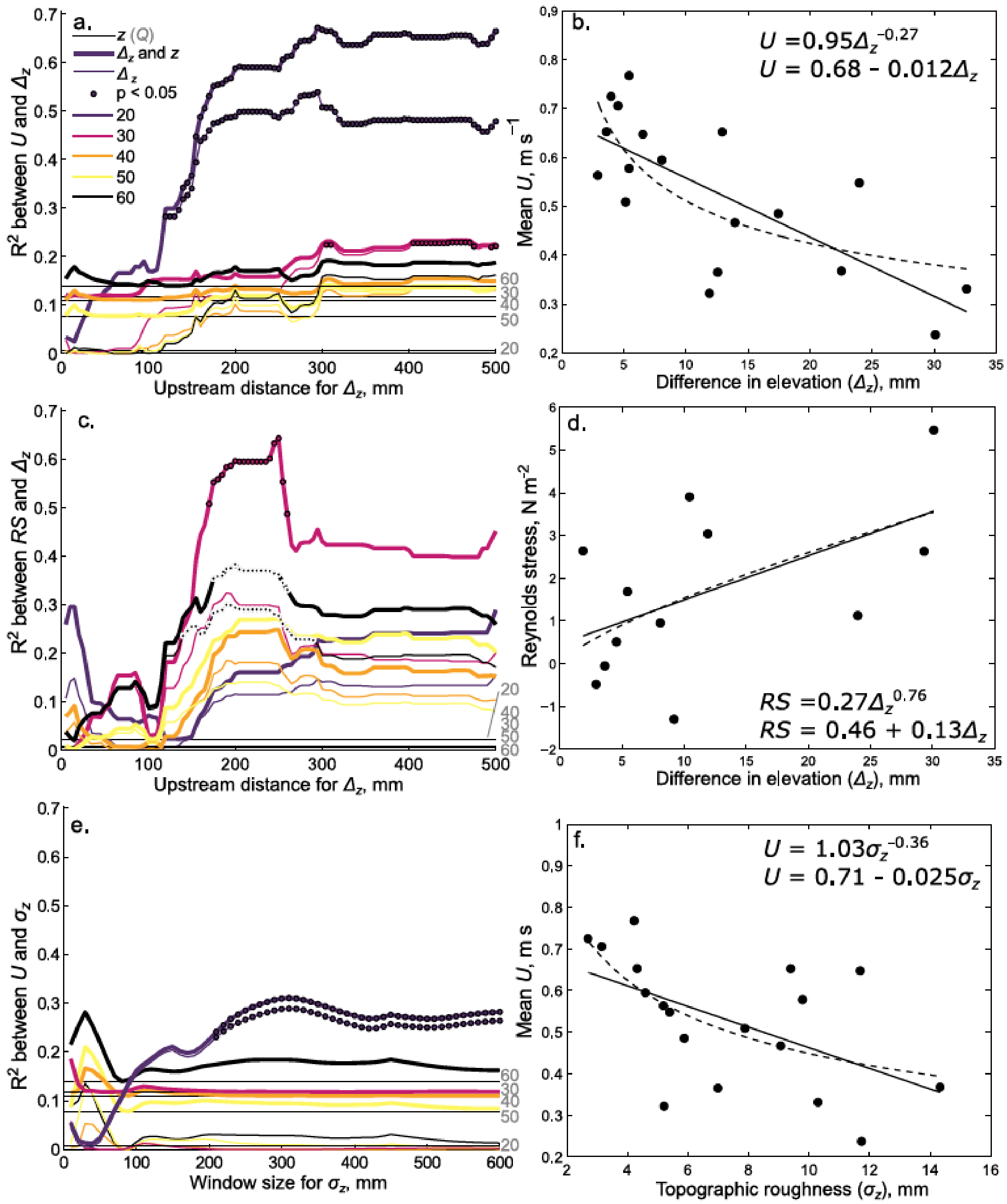

Figure 9: a) R^2 values for relationships between the upstream difference in surface elevations (Δ_z) and mean downstream velocity (U), using Δ_z calculated over a range of upstream distances. c) shows the same analysis, but for Reynolds stress (RS) instead of U. e) shows the same analysis as a), but characterising topography using the standard deviation of elevations (σ_z) within a square window centred on the velocity measurement location. In all of a), c) and e), thin lines are R^2 for the regression between the topographic index and the hydraulic data for each discharge; thick lines are R^2 for a regression that also incorporates the elevation of the measurement location (using the same colour scheme for Q), and dashed lines are for the regression between the point elevation and the hydraulic data. Circles

indicate statistically significant relationships ($p < 0.05$). b), d) and f) show the relationships between the topographic index and the hydraulic data for the highest R^2 in the previous panel. Dashed lines are power functions (top equation shown on each panel) and solid lines are linear relationships (bottom equation on each panel). In b) and f), $Q = 20\ l\ s^{-1}$, and in d) $Q = 30\ l\ s^{-1}$.

4.5. Impact of sediment on flow velocities

Flume runs where sediment was introduced and the ADV was in a single location (Figure 1d) illustrate the impact of sediment cover on downstream and vertical velocities (Figure 10). High sediment cover in the area upstream of the ADV (areal coverage proportion > 0.4) leads to a significant reduction in the mean downstream velocity (Figure 10a), and a less pronounced trend of reduction in vertical velocities (Figure 10b) and cross-stream velocities. With smaller amounts of sediment cover velocities tend to plot below the trend of data with no sediment cover (control run). In the absence of sediment some variation in the proportion of quadrant 2 and quadrant 4 events with changing discharge was reported above, but the amount of sediment cover seems to have little impact on this aspect of flow structure (Figure 10c).

The impact of sediment cover was evaluated using the difference between the velocity in each run with sediment cover and the control run with no sediment input. This difference was calculated for each of the points in Figure 10a, with velocities from the control series being interpolated at the appropriate discharge. Stepwise regression of this difference in velocity against discharge and proportion of sediment cover was performed for all three flow velocity components. In all three cases sediment cover contributed significantly to explaining the velocity difference ($p < 0.001$). Discharge was not a significant component ($p > 0.30$), which is not surprising as the changes in velocity with discharge measured in the control run have been removed from these data.

The formation of sediment cover changes the roughness of the bed upstream surrounding the ADV. The impact of this change was estimated by calculating a roughness length for this area of the bed (*i.e.* the area that sediment cover was calculated for) using the relationship:

$$k_{tot} = k_B F_e + k_A(1-F_e) \tag{4}$$

where k_{tot} is the total roughness length, k_A and k_B are the alluvial and bedrock roughness lengths respectively, and F_e is the fractional exposure of the channel bed [*Johnson*, 2014]. k_B is estimated as the standard deviation of surface elevations within this small area, which is 3.4 mm (compared to a channel-wide value of 12 mm). Although earlier analysis showed that Δ_z had a stronger correlation with velocity than σ_z, σ_z is used here because it is unclear what a comparable value of Δ_z for sediment cover would be, and for consistency with *Johnson* [2014]. k_A is estimated as 2 D_{50} [*Johnson*, 2014], which is 14.6 mm. k_{tot} is plotted against velocity in Figure 10d. In keeping with Figure 9f and previous hydraulic relationships, a power law was fitted. The exponent and coefficient are not significantly different to those fitted in Figure 9f, despite the fact that these are independent data sets, and with different ways of calculating the topographic roughness. Furthermore, although in both cases the exponent is significantly different from -1/6 at a 95% confidence level, this does not necessarily discount the use of Darcy-Weisbach relationships as simultaneous variations in local energy slope and depth have not been accounted for.

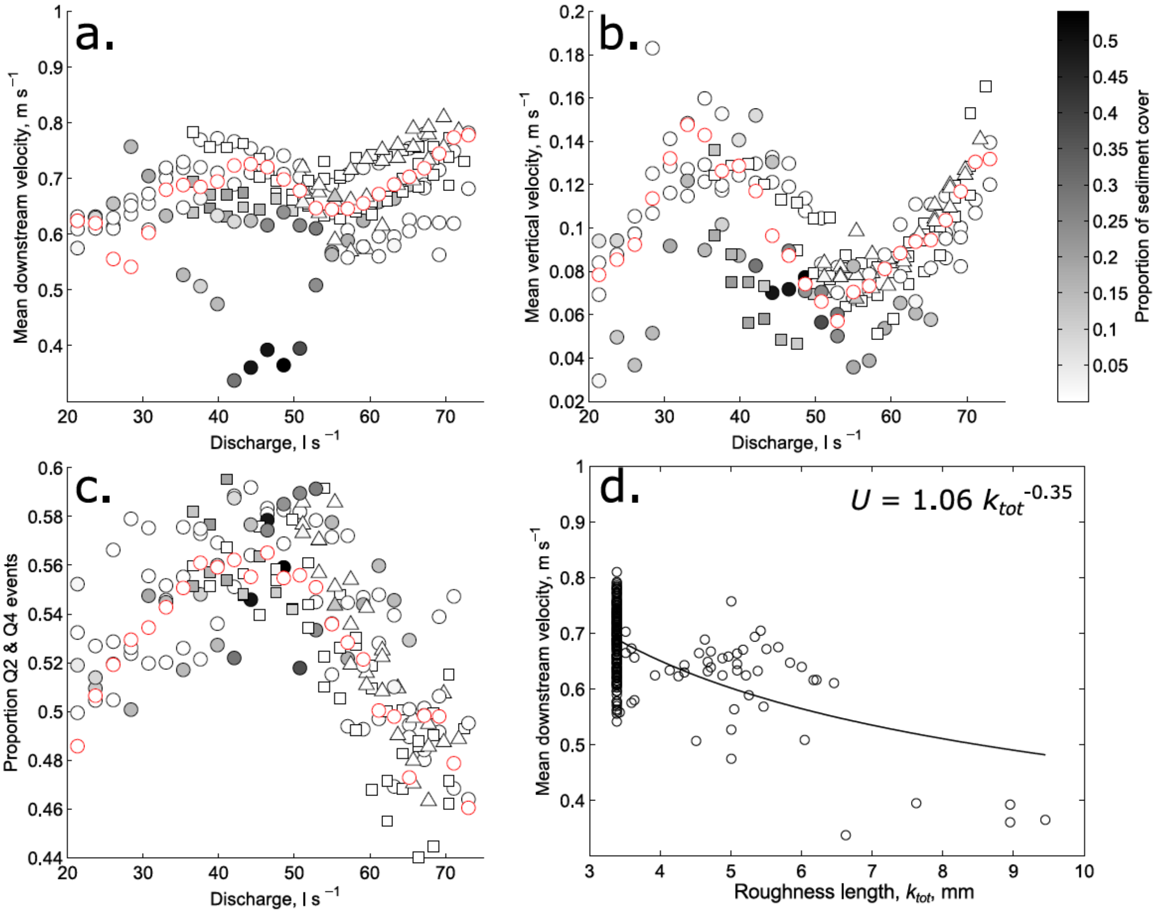

Figure 10: The impact of sediment cover on local velocities and flow structures; data are from all runs where sediment was introduced into the flume. The symbols show the discharge at which the run was initiated; o: 20 l s^{-1}, □: 35 l s^{-1}, Δ: 50 l s^{-1}.Figures show variation in a) downstream velocity, b) vertical velocity and c) proportion of time flow is in quadrants 2 and 4. Marker shade indicates the proportion of sediment cover in an area 40 x 50 mm upstream of the ADV location. Red markers are data from a control run with no sediment input. d) shows the relationship between k_{tot} (Equation 4) calculated from a linear combination of bedrock and sediment roughness lengths, and downstream velocity. The fitted power law has R^2 = 0.33 and the coefficient and exponent are significantly different to zero (p=0.05).

5. Discussion

In the discussion we address each of our research questions (Section 2.5), before considering the broader implications of our findings for bedrock-alluvial channels.

5.1. How do the spatial patterns of hydraulic properties change with discharge?

The channel topography induces considerable spatial variation in flow depth, velocity, Froude number and Reynolds stress (Figures 3, 5 and 6). As discharge increases, the range (and thus spatial variation) of flow depths remains approximately constant, whereas the range of velocities increases. At a single point, hydraulic properties can both increase and decrease as discharge increases. The scaled variability in velocities (Figure 4) remains largely unchanged throughout, although at the lowest discharge (20 l s^{-1}) the downstream velocities are significantly lower than at all other discharges. The vertical velocity component (Figure 4) shows a systematic trend of becoming less variable as discharge rises, whereas variability in the other components remains unchanged. When the spatial patterns of these changes are considered, a key result is the development of a core of high velocity and supercritical flow that links up all three measurement transects.

The development of a high velocity core is comparable to the hydraulic changes identified by *Richardson and Carling* [2006] in Birk Beck. They hypothesised that the channel switched from a macroturbulent mixing state (MMS) with complete mixing across the entire channel cross-section to a decoupled dead zone state (DDZS), with a decoupled core of faster flow. Aspects of the results presented here suggest that Trout Beck may behave in a similar manner. Between discharges of 20 and 40 l s^{-1}, the channel appears to be in an MMS. This is supported by the smaller variation in flow velocities at these discharges, and flow resistance (Darcy-Weisbach f) becoming independent of discharge at Q = 40 l s^{-1} (Figure 2d inset). Froude number also stabilises at just above unity at this discharge (Figure 3c). Between discharges of 40 and 50 l s^{-1}, the channel seems to transition into the DDZS, with the development of a core of supercritical flow and greater variation in velocity (Figure 5). However, even at the highest discharge there is still more lateral and downstream variation in Fr than was observed by *Tinkler* [1997], indicating that the bed topography is still influencing the flow.

The reason for this transition in our experiments seems to be a function of the differing response of the 3D flow field to the bed topography, and the changing scales of influence of the channel topography (discussed below). As the flume has smooth walls these changes do not result from the flow accessing additional roughness sources as has been postulated in the field [*Richardson and Carling*, 2006]. *Richardson and Carling* [2006] also identified two distinct thresholds, with the MMS developing above Q_1 when flow resistance decouples from discharge, and the DDZS occurring at the higher Q_2. In our experiments the decoupling of flow resistance occurred at around the same discharge as the development of the high velocity core, suggesting only a single threshold. However, the use of only five different discharges makes the identification of specific threshold difficult.

5.2. To what extent does local bed topography affect velocity?

The relatively poor correlation between bed elevation and downstream velocity (Figure 7b) is not surprising. However, analysis of the correlations between downstream velocity (U) and Reynolds stress and indices of local bed topography (Δ_z and σ_z) shows that at some discharges upstream bed elevations do affect downstream velocity. At the lowest discharge, Q = 20 l s^{-1}, there is a significant relationship between both Δ_z and σ_z and U, with the strongest relationship when Δ_z and σ_z are calculated over a distance of about 300 mm. At other discharges the relationship between Δ_z or σ_z and U is at best similar to the weak relationship between the local bed elevation (z) and U, with relationships calculated using σ_z being worse.

The velocity therefore seems to be conditioned by the upstream bed topography at low discharges, but not at larger discharges. This is consistent with the normalised flow data (Figure 4a), in which values of U/U^* are significantly lower at 20 l s^{-1} than at higher discharges, suggesting an increased flow resistance at the lower discharge. Values of RMS_z/U^* show that there is also more vertical turbulence in the flow at the lowest discharge, suggesting that the higher flow resistance is caused by the development of larger coherent flow structures downstream of topographic steps that increase vertical flow and reduce downstream velocities. Consistent with these data, *Hardy et al.* [2010] found, over an alluvial bed, that at lower relative roughness (i.e. increased flow depth for a fixed bed topography) flow structures became less defined throughout the flow depth, and the reduction in downstream velocity was less pronounced. This hydraulic state is also consistent with the MMS of *Richardson and Carling* [2006].

The identified length scale of 300 mm (3 m in the field) is likely to reflect the length of this detachment zone behind the dominant steps in the bed. Observations suggest that pebble clusters can influence the flow over a downstream distance equivalent to 3.5 times the obstacle height [*Brayshaw et al.*, 1983; *Lawless and Robert*, 2001; *Lacey and Roy*, 2008]. Applying the 3.5 scaling factor to our site suggests that a length scale of 300 mm corresponds with an obstacle height of 86 mm (860 mm field), which is comparable to some of the larger steps in the bed topography. The relationship between Reynolds stress and the topographic indices is harder to explain, with significant correlations only at 30 and 60 l s^{-1}. This therefore demonstrates that the different components of velocity do not appear to respond in the same way to the identified topographic indices.

5.3. How do sediment patches affect local hydraulics?

Experiments with sediment demonstrated that sediment cover alters the local hydraulics, decreasing downstream flow velocities. The relationship proposed by *Johnson* [2014] for estimating the topographic roughness of mixed bedrock-alluvial surfaces was used to predict how roughness in the region affecting the velocity recorded by the ADV changed as sediment cover developed. The resulting relationship between downstream velocity and topographic roughness (Figure 10d) has a very similar form to the relationship derived from clear water flows (Figure 9f), with both power law exponents being about -0.35. This provides support for the relationship proposed by *Johnson* [2014], albeit maybe as a power function. Both relationships are different to either the linear or -1/6 power suggested by the Manning's and Darcy-Weisbach relationships, however concurrent variations in local energy slope and depth were not accounted for. Further analysis of the runs with sediment cover, such as the calculation of flow resistance parameters from the flow data, was not possible because local water depths were not recorded.

The above analysis was limited to a single ADV location and results may vary spatially. The σ_z in the ADV measurement location was 3.4 mm, which is comparatively smooth compared to sediment D_{50} of 7.3 mm. Mean values of σ_z across the entire channel range from 5 to 6 mm over window sizes of 150 to 300 mm (Figure 8). Thus there is a significant proportion of the channel where adding sediment could decrease topographic roughness by infilling bedrock depressions, so potentially increasing local flow velocities.

5.4. Implications for bedrock-alluvial channels

These experiments have demonstrated relationships between spatial patterns of flow (velocity, Froude number and Reynolds stress), bed topography (including the impact of sediment cover), and discharge. However, these experimental results are for one 18 m long section of a particular bedrock-alluvial channel, and so it is necessary to consider possible implications for bedrock-alluvial rivers in general. The topography of this reach of Trout Beck is relatively low relief, with an elevation range of just over 1 m (excluding the net downstream slope), and a blocky topography which becomes less rough towards the downstream end of the reach. Although such topography is not unusual in bedrock-alluvial channels, the value of our results also lies in the validation of concepts that have either only been observed at a single site, or have not previously been tested. In particular we have demonstrated: 1) increased spatial variation in flow characteristics with discharge, which is not driven by channel bank roughness; and, 2) that at the lowest discharge, velocity is correlated with upstream bed topography.

The changes in spatial flow conditions and relatively poor relationships between topographic roughness and hydraulics at most discharges have implications for predicting hydraulics in bedrock-alluvial rivers. The increased variation and development of a high velocity core mean that the distribution of shear stress over the bed will be highly spatially variable. Furthermore, Reynolds stress shows different spatial variation to other hydraulic parameters. The location of the high velocity core will have implications for the pathways that bedload will be transported along, the areas of the bed that will be most subject to erosional processes, and the deposition and erosion of sediment patches (see companion paper).

The analysis comparing topographic indices and velocity suggests that Δ_z and σ_z can be used to quantify the impact of the topography on the flow at some, but not all, discharges. The analysis also supports the use of a mixing model approach for combining sediment and bedrock roughness. There is also the question of the most appropriate window size for calculating Δ_z and σ_z. For any given river, this length scale is likely to be a function of the bed topography and may change as a function of discharge. One possible approach is to use a length scale that is a function of the topographic relief, for example a length of 3.5 times a representative step height as suggested from our data and the effect of particle clusters on hydraulics. The second approach is to look at the changing distribution of σ_z with increasing window size, and to identify a minimum window size that is needed to capture the topographic variability.

6. Conclusions

A Froude-scaled model of a bedrock-alluvial river reach was used to quantify how flow hydraulics changed across a range of discharges, and how they related to the bed topography. The flume experiments demonstrated that: 1) spatial variation in flow velocity, Froude number and Reynolds stress increases with discharge; 2) flow resistance and Froude number become independent of discharge at higher discharges; 3) local flow velocity and Reynolds stress are correlated with the range of local bed topography at some, but not most, discharges; and, 4) sediment cover produces changes in flow velocity that are consistent with predicted changes in surface roughness. Although these data are from a single channel, they have wider implications. In particular, the results indicate that there is no single representative roughness length for a bedrock-alluvial channel, with topographic analysis showing that standard deviation of surface elevations does not converge to a single value over length scales up to the width of the flume (channel width at field scale), and that different hydraulic properties correlate with local topography at only some discharges. The results also indicate that the transition from a macroturbulent mixing state to a decoupled dead zone state, as observed by *Richardson and Carling* [2006], may be a characteristic behaviour of bedrock-alluvial channels, and also that bank roughness is not necessary for this transition to occur.

The hydraulics of bedrock-alluvial channels remain little researched, despite their importance for bedload transport, channel incision and ultimately landscape evolution. The implications of the role of hydraulics for the development and erosion of sediment cover in this reach are addressed in the companion paper. To extend the findings in this paper further, high-resolution, data on spatially distributed hydraulics are required (either from scaled models or the field),from bedrock-alluvial channels with a wide range of channel morphologies and extents of sediment cover. Such datasets would enable more robust relationships between hydraulics and bed topography, and the way in which the relationships change with discharge, to be established.

Acknowledgements

This project was supported by a Royal Geographical Society (with IBG) Small Research Grant to RAH. Thanks to Bishnu Sharma and Rob Ferguson for flow data from Trout Beck and for the high flows extrapolation, and to Kenny Roberts and Tim Montgomery for laboratory assistance. The authors acknowledge the thorough and useful comments of the editors, Phairot Chatanantavet, Jeff Peakall and Tim Davies. Data are available from the corresponding author by request.

References

Babaeyan-Koopaei, K., D. Ervine, P. Carling, and Z. Cao (2002), Velocity and Turbulence Measurements for Two Overbank Flow Events in River Severn, J. Hydraul. Eng., 128(10), 891–900, doi:10.1061/(ASCE)0733-9429(2002)128:10(891).

Baynes, E. R. C., M. Attal, S. Niedermann, L. A. Kirstein, A. J. Dugmore, and M. Naylor (2015), Erosion during extreme flood events dominates Holocene canyon evolution in northeast Iceland, PNAS, 201415443, doi:10.1073/pnas.1415443112.

Brayshaw, A. C., L. E. Frostick, and I. Reid (1983), The hydrodynamics of particle clusters and sediment entrapment in coarse alluvial channels, Sedimentology, 30(1), 137–143, doi:10.1111/j.1365-3091.1983.tb00656.x.

Buffin-Bélanger, T., S. Rice, I. Reid, and J. Lancaster (2006), Spatial heterogeneity of near-bed hydraulics above a patch of river gravel, Water Resour. Res., 42(4), W04413, doi:10.1029/2005WR004070.

Chatanantavet, P., and G. Parker (2008), Experimental study of bedrock channel alluviation under varied sediment supply and hydraulic conditions, Water Resour. Res., 44(12), doi:10.1029/2007WR006581.

Coleman, S. E., V. I. Nikora, and J. Aberle *(*2011*)*, Interpretation of alluvial beds through bed-elevation distribution moments, Water Resour. Res., 47*, W11505, doi:*10.1029/2011WR010672.

Colombini, M. (1993), Turbulence-driven secondary flows and formation of sand ridges, J. Fluid Mech., 254, 701–719, doi:10.1017/S0022112093002319.

Cook, K. L., J. M. Turowski, and N. Hovius (2013), A demonstration of the importance of bedload transport for fluvial bedrock erosion and knickpoint propagation, Earth Surf. Process. Landforms, 38(7), 683–695, doi:10.1002/esp.3313.

Doroudian, B., F. Bagherimiyab, and U. Lemmin (2010), Improving the accuracy of four-receiver acoustic Doppler velocimeter (ADV) measurements in turbulent boundary layer flows, Limnol. Oceanogr. Meth., 8, 575–591, doi:10.4319/lom.2010.8.575.

Elder K, Kattelmann R, and R. Ferguson (1990). Refinements in dilution gauging for mountain streams. Int. Assoc. Hydrol. Sci. Publ. 193, 247-254.

Ferguson, R. I. (2012), River channel slope, flow resistance, and gravel entrainment thresholds, Water Resour. Res., 48(5), W05517, doi:10.1029/2011WR010850.

Finnegan, N. J., L. S. Sklar, and T. K. Fuller (2007), Interplay of sediment supply, river incision, and channel morphology revealed by the transient evolution of an experimental bedrock channel, J. Geophys. Res., 112(F3), doi:10.1029/2006JF000569.

Grant, G. E. (1997), Critical flow constrains flow hydraulics in mobile-bed streams: A new hypothesis, Water Resour. Res., 33(2), 349–358, doi:10.1029/96WR03134.

Gupta, A., and H. Fox (1974), Effects of high-magnitude floods on channel form: A case study in Maryland Piedmont, Water Resour. Res., 10(3), 499–509, doi:10.1029/WR010i003p00499.

Hardy, R.J., Best, J.L., Lane, S.N., and P.E. Carbonneau (2010), Coherent flow structures in a depth-limited flow over a gravel surface: The influence of surface roughness, J. Geophys. Res. 115, F03006. doi:10.1029/2009JF001416

Heritage, G. L., B. P. Moon, L. J. Broadhurst, and C. S. James (2004), The frictional resistance characteristics of a bedrock-influenced river channel, Earth Surf. Process. Landforms, 29(5), 611–627, doi:10.1002/esp.1057.

Huang, H. Q., H. H. Chang, and G. C. Nanson (2004*)*, Minimum energy as the general form of critical flow and maximum flow efficiency and for explaining variations in river channel pattern, Water Resour. Res., 40, *W04502*, *doi:*10.1029/2003WR002539.

Inoue, T., N. Izumi, Y. Shimizu, and G. Parker (2014), Interaction among alluvial cover, bed roughness and incision rate in purely bedrock and alluvial-bedrock channel, J. Geophys. Res. Earth Surf., 2014JF003133, doi:10.1002/2014JF003133.

Jansen, J. D., D. Fabel, P. Bishop, S. Xu, C. Schnabel, and A. T. Codilean (2011), Does decreasing paraglacial sediment supply slow knickpoint retreat?, Geology, 39(6), 543–546, doi:10.1130/G32018.1.

Johnson, J. P. L. (2014), A surface roughness model for predicting alluvial cover and bed load transport rate in bedrock channels, J. Geophys. Res. Earth Surf., 2013JF003000, doi:10.1002/2013JF003000.

Johnson, J. P. L., and K. X. Whipple (2010), Evaluating the controls of shear stress, sediment supply, alluvial cover, and channel morphology on experimental bedrock incision rate, J. Geophys. Res., 115, F02018, doi:201010.1029/2009JF001335.

Johnson, J. P., and K. X. Whipple (2007), Feedbacks between erosion and sediment transport in experimental bedrock channels, Earth. Surf. Proc. Land., 32(7), 1048–1062, doi:10.1002/esp.1471.

Lacey, R. W. J., and A. G. Roy (2008), The spatial characterization of turbulence around large roughness elements in a gravel-bed river, Geomorphology, 102(3–4), 542–553, doi:10.1016/j.geomorph.2008.05.045.

Lane, S. N., P. M. Biron, K. F. Bradbrook, J. B. Butler, J. H. Chandler, M. D. Crowell, S. J. McLelland, K. S. Richards, and A. G. Roy (1998), Three-dimensional measurement of river channel flow processes using acoustic doppler velocimetry, Earth Surf. Process. Landforms, 23(13), 1247–1267, doi:10.1002/(SICI)1096-9837(199812)23:13<1247::AID-ESP930>3.0.CO;2-D.

Lawless, M., and A. Robert (2001), Three-dimensional flow structure around small-scale bedforms in a simulated gravel-bed environment, Earth Surf. Process. Landforms, 26(5), 507–522, doi:10.1002/esp.195.

Legleiter, C. J., T. L. Phelps, and E. E. Wohl (2007), Geostatistical analysis of the effects of stage and roughness on reach-scale spatial patterns of velocity and turbulence intensity, Geomorphology, 83(3–4), 322–345, doi:10.1016/j.geomorph.2006.02.022.

Leopold, L. B., and T. Maddock Jr. (1953), The hydraulic geometry of stream channels and some physiographic implications, USGS Professional Paper 252, 57 pp.

Martin, V., T. S. R. Fisher, R. G. Millar, and M. C. Quick (2002), ADV Data Analysis for Turbulent Flows: Low Correlation Problem, Hydraulic Measurements and Experimental Methods, pp. 1–10, American Society of Civil Engineers. doi: 10.1061/40655(2002)101

Milan, D. J. (2012), Geomorphic impact and system recovery following an extreme flood in an upland stream: Thinhope Burn, northern England, UK, Geomorphology, 138(1), 319–328, doi:10.1016/j.geomorph.2011.09.017.

Montgomery, D. R., T. B. Abbe, J. M. Buffington, N. P. Peterson, K. M. Schmidt, and J. D. Stock (1996), Distribution of bedrock and alluvial channels in forested mountain drainage basins, Nature, 381(6583), 587–589, doi:10.1038/381587a0.

Peakall, J., Ashworth, P.J., Best, J., 1996. Physical modelling in fluvial geomorphology: Principles, applications and unresolved issues. In: The Scientific Nature of Geomorphology, (Eds.) Rhoads, B.L. and Thorn, C.E., 221-253.

Richardson, K., and P. A. Carling (2006), The hydraulics of a straight bedrock channel: Insights from solute dispersion studies, Geomorphology, 82(1–2), 98–125, doi:10.1016/j.geomorph.2005.09.022.

Schumm, S. A., and R. W. Lichty (1965), Time, space, and causality in geomorphology, Am J Sci, 263(2), 110–119, doi:10.2475/ajs.263.2.110.

Strom, K., and A. Papanicolaou (2007), ADV Measurements around a Cluster Microform in a Shallow Mountain Stream, J. Hydraul. Eng., 133(12), 1379–1389, doi:10.1061/(ASCE)0733-9429(2007)133:12(1379).

Thompson, D., and E. Wohl (1998), Flume Experimentation and Simulation of Bedrock Channel Processes, in Rivers Over Rock: Fluvial Processes in Bedrock Channels, edited by K. J. Tinkler and E. E. Wohl, pp. 279–296, American Geophysical Union.

Tinkler, K. J. (1997), Critical flow in rockbed streams with estimated values for Manning's n, Geomorphology, 20(1–2), 147–164, doi:10.1016/S0169-555X(97)00011-1.

Tinkler, K., and E. Wohl (1998), A Primer on Bedrock Channels, in Rivers Over Rock: Fluvial Processes in Bedrock Channels, edited by K. J. Tinkler and E. E. Wohl, pp. 1–18, American Geophysical Union.

Turowski, J. M., and D. Rickenmann (2009), Tools and cover effects in bedload transport observations in the Pitzbach, Austria, Earth Surf. Process. Landforms, 34(1), 26–37, doi:10.1002/esp.1686.

Turowski, J. M., N. Hovius, A. Wilson, and M.-J. Horng (2008), Hydraulic geometry, river sediment and the definition of bedrock channels, Geomorphology, 99(1-4), 26–38, doi:10.1016/j.geomorph.2007.10.001.

Van, T. P. D., P. A. Carling, and P. M. Atkinson (2012), Modelling the bulk flow of a bedrock-constrained, multi-channel reach of the Mekong River, Siphandone, southern Laos, Earth Surf. Process. Landforms, 37(5), 533–545, doi:10.1002/esp.2270.

Venditti, J. G., C. D. Rennie, J. Bomhof, R. W. Bradley, M. Little, and M. Church (2014), Flow in bedrock canyons, Nature, 513(7519), 534–537, doi:10.1038/nature13779.

Wahl, T. L. (2000), Analyzing ADV Data Using WinADV, Building Partnerships, pp. 1–10, American Society of Civil Engineers. doi: 10.1061/40517(2000)300

Wells, S. G., and A. M. Harvey (1987), Sedimentologic and geomorphic variations in storm-generated alluvial fans, Howgill Fells, northwest England, Geol. Soc. Am. Bull., 98(2), 182–198, doi:10.1130/0016-7606(1987)98<182:SAGVIS>2.0.CO;2.

Whipple, K. (2004), Bedrock rivers and the geomorphology of active orogens, Annu. Rev. Earth Planet. Sci., 32, 151–185, doi:10.1146/annurev.earth.32.101802.120356.

Whitbread, K., J. Jansen, P. Bishop, and M. Attal (2015), Substrate, sediment, and slope controls on bedrock channel geometry in postglacial streams. J. Geophys. Res. Earth Surf., 120, 779–798. doi: 10.1002/2014JF003295.

Wohl, E., and G. C. L. David (2008), Consistency of scaling relations among bedrock and alluvial channels, J. Geophys. Res., 113(F4), F04013, doi:10.1029/2008JF000989.

Wohl, E. E., D. M. Thompson, and A. J. Miller (1999), Canyons with undulating walls, Geol. Soc. Am. Bull., 111(7), 949–959, doi:10.1130/0016-7606(1999)111<0949:CWUW>2.3.CO;2.

Young, W.J. and Warburton, J. (1996) Principles and practice of hydraulic modelling of braided gravel-bed rivers, J. Hydrol (NZ), 52, 175-98.